ACS APPLIED MATERIALS & INTERFACES

Research Article

www.acsami.org

Improving the Conductivity of PEDOT:PSS Hole Transport Layer in Polymer Solar Cells via Copper(II) Bromide Salt Doping

Zhiqiang Zhao,[†] Qiliang Wu,[†] Fei Xia,[†] Xiang Chen,[†] Yawei Liu,[†] Wenfeng Zhang,[†] Jun Zhu,[‡] Songyuan Dai,[‡] and Shangfeng Yang*[,†]

[†]Hefei National Laboratory for Physical Sciences at Microscale, CAS Key Laboratory of Materials for Energy Conversion, Department of Materials Science and Engineering, Synergetic Innovation Center of Quantum Information & Quantum Physics, University of Science and Technology of China (USTC), Hefei 230026, China

[‡]Key Laboratory of Novel Thin Film Solar Cells, Institute of Plasma Physics, Chinese Academy of Sciences, Hefei 230031, China

Supporting Information

ABSTRACT: Copper(II) bromide ($CuBr_2$) salt has been applied to dope poly(3,4-ethylene dioxythiophene):poly(styrenesulfonate) (PEDOT:PSS) as the hole transport layer (HTL) in polymer solar cells (PSCs), improving dramatically the conductivity of PEDOT:PSS film and consequently the device power conversion efficiency (PCE). Under the optimized doping concentration of $CuBr_2$ of 10 mmol·L^{-1}, PCE of the $CuBr_2$:PEDOT:PSS HTL-incorporated BHJ-PSC device based on poly[*N*-9″-hepta-decanyl-2,7-carbazole-*alt*-5,5-(4′,7′-di-2-thienyl-2′,1′,3′- benzothiadiazole) (PCDTBT) and [6,6]-phenyl C71-butyric acid methyl ester ($PC_{71}BM$) (PCDTBT:$PC_{71}BM$) reaches 7.05%, which is improved by ∼20.7% compared to that of the reference device based on pristine PEDOT:PSS HTL (5.84%) and represents the highest PCE for PCDTBT:$PC_{71}BM$-based PSC devices without an electron transport layer (ETL) reported so far. The dramatic improvement of the conductivity of PEDOT:PSS film is interpreted by the weakening of the Coulombic attractions between PEDOT and PSS components. The work function of $CuBr_2$:PEDOT:PSS slightly increases compared to that of the undoped PEDOT:PSS as inferred from scanning Kelvin probe microscopy (SKPM) measurements, contributing to the improved PCE due to the increases of the open-current voltage (V_{oc}) and fill factor (FF).

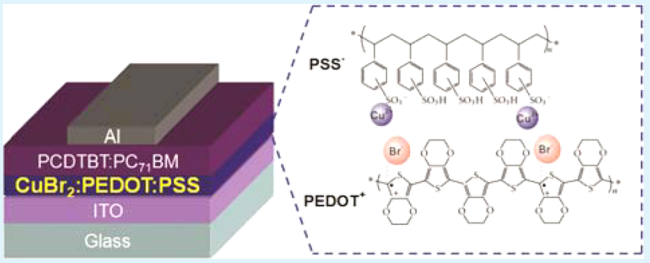

KEYWORDS: *polymer solar cells, hole transport layer, PEDOT:PSS, copper bromide, conductivity*

INTRODUCTION

As a promising renewable energy source, polymer solar cells (PSCs) have been attracting great attention during the past two decades because of their advantages of low-cost manufacturing, light weight, high flexibility, and easy roll-to-roll fabrication.[1−7] The most popular and efficient architecture for PSCs is bulk heterojunction (BHJ) structure comprising an interpenetrating network of a conjugated polymer donor and a soluble fullerene acceptor as the photoactive layer and either conventional or inverted BHJ-configurations has been established.[2−5] For the state-of-the-art solution-processable BHJ-PSCs, the recent advances in the synthesis of novel conjugated polymer donors and fullerene acceptors as well as interface engineering contribute to a high power conversion efficiency (PCE) approaching 10%.[3,8−10] Further improvement of PCE is highly desired to meet the requirement for commercialization of PSCs, and this can be realized by a practical approach to optimize the device structure, especially the interfaces between donor(acceptor)/electrodes, which is more facile than synthesizing new photoactive materials with improved photovoltaic properties.[3,11−17]

The interfaces between donor(acceptor)/electrodes are generally determinative for efficient charge transport and extraction for a given donor:acceptor BHJ-PSC device.[3,12,15−18] To improve such interfaces, interfacial layers or buffer layers including hole transport layers (HTLs) and/or electron transport layers (ETLs) are usually introduced between the active layer and the electrodes, which may facilitate charge collection and extraction via inducing interfacial charge redistribution, geometry modifications, and/or chemical reactions.[3,9,11,16,18] In particular, HTL materials for PSCs that are introduced between the active layer and the anode have been extensively studied in recent years and demonstrated to benefit selectively transporting holes and blocking electrons.[19] To date, the reported HTL materials include poly(3,4-ethylene dioxythiophene):poly(styrenesulfonate) (PEDOT:PSS),[5,15,20,21] semiconducting metal oxides such as MoO_x,[16,22,23] conjugated or nonconjugated polymers and small-molecule organic materials, self-assembled monolayers,

Received: August 12, 2014
Accepted: December 23, 2014
Published: December 23, 2014

DOI: 10.1021/am505387q
ACS Appl. Mater. Interfaces 2015, 7, 1439−1448

and graphene oxides.[4,24−27] Among them, PEDOT:PSS has been the most widely used HTL for conventional PSCs since the late 1990s, being effective in transporting holes to the anode and blocking electrons.[19,28] PEDOT:PSS is advantageous in terms of its high optical transparency in the visible light spectrum, easy aqueous solution processing, high work function (4.8−5.2 eV as usually reported) facilitating the formation of an Ohmic contact with many common polymer donors, with which PEDOT:PSS behaves as a good HTL meeting the requirements of HTL materials.[15,19,28−30] However, the pristine PEDOT:PSS HTL film usually suffers from a very low conductivity (<1 S·cm^{-1}) because of the existence of an insulating PSS moiety essential for the formation of aqueous dispersion required for solution processing.[15,29,31] Indeed, in an early study it was reported that the application of a relatively thick PEDOT:PSS HTL in poly(2-methoxy-5-(3′,7′-dimethyloctyloxy)-1,4-phenylene-vinylene) (MDMO-PPV) and [6,6]-phenyl-C61-butyric acid methyl ester ($PC_{61}BM$) BHJ-PSCs resulted in a decrease of both short-circuit current (J_{sc}) and fill factor (FF) along with the increase of the series resistance (R_s) due to the high resistivity of PEDOT:PSS film.[32] Therefore, increasing the conductivity of PEDOT:PSS appears to be essential for improving hole transport, and two major approaches have previously been developed to increase the conductivity of PEDOT:PSS film which is consequently applied in ITO-free PSCs. One is to dope the aqueous PEDOT:PSS solution with small-molecule organic compounds such as polar solvents (*N*,*N*-dimethylformamide (DMF), dimethyl sulfoxide (DMSO), ethylene glycol, diethylene glycol, D-sorbitol etc.), ionic liquid, anionic surfactant, or dimethyl sulfate.[15,19,20,33−36] Another approach is based on a "dipping" post-treatment of the PEDOT:PSS films with polar organic compounds, zwitterion, surfactant, inorganic salts, carboxylic or inorganic acid, sulfuric acid (H_2SO_4), etc.[20,29,31,37−39] While both treatments (doping or dipping) typically led to dramatic improvement of the conductivity of PEDOT:PSS film which is required for ITO-free PSCs, in some cases the performance of PSC devices based on treated PEDOT:PSS films can be deteriorated.[29,37,39] For instance, when the PEDOT:PSS (Clevios P) film was post-treated by inorganic salts such as copper(II) chloride ($CuCl_2$) and copper(II) bromide ($CuBr_2$) via "dipping" post-treatment, i.e., dropping the aqueous solution of salt onto the PEDOT:PSS film under heating at 140 °C, the conductivity of PEDOT:PSS film increased by a factor of about 700 and more than 1000 for $CuCl_2$ and $CuBr_2$, respectively. This was higher than that treated by zwitterions. However, the efficiency of ITO-free BHJ-PSC device based on $CuCl_2$ ($CuBr_2$)-treated PEDOT:PSS film anode was lower than that based on zwitterions-treated one. This phenomenon was interpreted by the presence of small anions in PEDOT:PSS film as evidenced by the high dark current and possible migration of metal cations to the active layer.[29] Thus, an open question that needs to be addressed is whether the presence of metal cations and anions in bulk PEDOT:PSS film would deteriorate the performance of PSC if the inorganic salt dopes aqueous PEDOT:PSS solution prior to film fabrication.

In this paper, we report the application of $CuBr_2$ salt in doping aqueous PEDOT:PSS solution, resulting in dramatically improved conductivity of PEDOT:PSS film and consequently PCE of the BHJ-PSC device, in which a low band gap donor poly[*N*-9″-hepta-decanyl-2,7-carbazole-*alt*-5,5-(4′,7′-di-2-thienyl-2′,1′,3′-benzothiadiazole) (PCDTBT) and [6,6]-phenyl C71-butyric acid methyl ester ($PC_{71}BM$) (PCDTBT:$PC_{71}BM$) were used in the active layer. The effects of $CuBr_2$ doping on the conductivity, composition, and morphology of PEDOT:PSS film were investigated, and the mechanism for the efficiency enhancement upon $CuBr_2$ doping was discussed.

EXPERIMENTAL SECTION

Materials. The indium tin oxide (ITO) glass substrate with a sheet resistance of 8 Ω/sq was purchased from Shenzhen Nan Bo Group, China. PEDOT:PSS (Clevios P Al4083) was purchased from SCM Industrial Chemical Co., Ltd., for which the PEDOT:PSS concentration is 1.3% by weight and the weight ratio of PSS to PEDOT is 6:1. PCDTBT and $PC_{71}BM$ were bought from Solarmer Material Inc. and Solenne B.V., respectively. $CuBr_2$ was purchased from Sinopharm Chemical Reagent Co., Ltd. All chemicals were used as received without further purification.

Device fabrication. Our detailed fabrication procedure of the P3HT:PCBM BHJ-PSCs has been reported previously.[11,18,37,40−42] In brief, the ITO-coated glass substrate was first cleaned with detergent, then ultrasonicated in acetone and isopropanol, and subsequently dried in an oven overnight. PEDOT:PSS aqueous solution was first filtered by a 0.45 μm polyvinyl difluoride syringe filter. $CuBr_2$ was then added into the PEDOT:PSS aqueous solution with variable concentrations (5−15 mmol·L^{-1}), and the $CuBr_2$:PEDOT:PSS blend solution was ultrasonicated for 5−10 min and stored at about 4 °C in a refrigerator prior to film fabrication. The precleaned ITO glasses were subsequently treated by ozone−ultraviolet for 12 min. A thin film of $CuBr_2$:PEDOT:PSS (32 ± 2 nm thick, see Supporting Information Figure S1) was spin-coated onto the ITO surface at 3000 rpm for 60 s and then annealed at 120 °C for 30 min in air. Pristine (undoped) PEDOT:PSS film was also prepared under identical conditions for comparison. The PCDTBT:$PC_{71}BM$ (1:4 w/w) active blend was dissolved in chlorobenzene:dichlorobenzene (1:3 v/v) mixed solvents by stirring at 50 °C overnight.[43] This blend solution was spin-coated on the top of $CuBr_2$:PEDOT:PSS film at 2500 rpm for 60 s in air to form a thin active layer with a thickness of ∼70 nm. All of the solution processes and film preparation were carried out in air atmosphere. Finally, the device was transferred into a vacuum chamber (∼10^{-5} Torr), and an Al electrode (about 80 nm thick) was thermally deposited onto the active layer through a shadow mask to define the effective active area of the devices (2 × 7 mm^2).

Measurements and Characterization. The sheet resistance of $CuBr_2$:PEDOT:PSS film was measured by using a four-point probe technique with a source measurement unit (Keithley 2400). The thickness of the film was measured by a KLA-Tencor P6 surface profilometer. Transmittance was obtained using a UV−vis−NIR spectrophotometer (UV-3600, Shimadzu, Japan). X-ray photoelectron spectroscopy (XPS) was performed using an ESCALAB 250 X-ray photoelectron spectrometer. Raman spectroscopy was obtained by using a Renishaw inVia Raman microscope. Atomic force microscopy (AFM) measurements were carried out on a Veeco DI-Multimode V scanning probe microscope using tapping mode. Scanning Kelvin probe microscopy (SKPM) measurements were carried out on the same microscope using SKPM mode. All samples were measured by the same tip to avoid any change in the tip's work function. A standard HOPG measurement was done as a reference prior to the measurement of each sample so as to avoid the possible variation resulting from the tip and the atmosphere.

The current density−voltage (*J*−*V*) characterization of BHJ-PSCs was carried out by using a Keithley 2400 source measurement unit under simulated AM 1.5 irradiation (100 mW·cm^{-2}) with a standard xenon-lamp-based solar simulator (Oriel Sol 3A, USA). The solar simulator illumination intensity was calibrated by a monocrystalline silicon reference cell (Oriel P/N 91150 V, with KG-5 visible color filter) calibrated by the National Renewable Energy Laboratory (NREL). The measurement parameters are set as follows: pre sweep delay, 0.5 s; bias direction, forward; max reverse bias, −0.1 V; max forward bias, 1.0 V; number sweep points, 100; dwell time, 30 ms. All the measurements were carried out in air, and a mask with a well-defined area size of 14.0 mm^2 was attached onto the cell to define the

DOI: 10.1021/am505387q
ACS Appl. Mater. Interfaces 2015, 7, 1439−1448

effective area so as to ensure accurate measurement and to avoid the so-called "edge effect".[44] More than 10 devices were fabricated and measured independently under each experimental condition to ensure the consistency of the data. The average data as well as the best performance were used in the following discussions. To measure the stability of the device, the device was stored in a glovebox with the concentrations of H_2O and O_2 lower than 1 ppm, and PCE was measured in ambient condition with an interval of 0.5 day.

RESULTS AND DISCUSSION

Effects of $CuBr_2$ Doping on the Electrical and Optical Properties of the PEDOT:PSS Film. As reported in the literature, when the PEDOT:PSS films were "dipping" post-treated by inorganic salts including $CuCl_2$, $CuBr_2$, and $InCl_3$ via dropping the aqueous solution of salts onto the PEDOT:PSS films heated at 140 °C, the conductivity of PEDOT:PSS film was improved by 2−3 orders of magnitude.[31,38] This conductivity enhancement was attributed to not only the PSS loss from the PEDOT:PSS blend film but also to the conformational change of PEDOT moieties resulted from the ion-induced screening effect of the charges on PEDOT and PSS.[31,38] In such studies, PEDOT:PSS (Clevios P) with a relatively higher conductivity instead of PEDOT:PSS (Clevios P Al4083) was used, and the as-prepared PEDOT:PSS film was treated by dropping the salt solution onto its surface instead of doping in bulk phase; thus, the influence of salts on PEDOT:PSS film was fulfilled by interfacial interactions.[38] It is thus intuitive to investigate whether salt doping in bulk phase of low-conductivity PEDOT:PSS (Clevios P Al4083) film will improve the conductivity of PEDOT:PSS film. The conductivities of PEDOT:PSS (Clevios P Al4083) films with and without $CuBr_2$ doping are compared in Figure 1. The

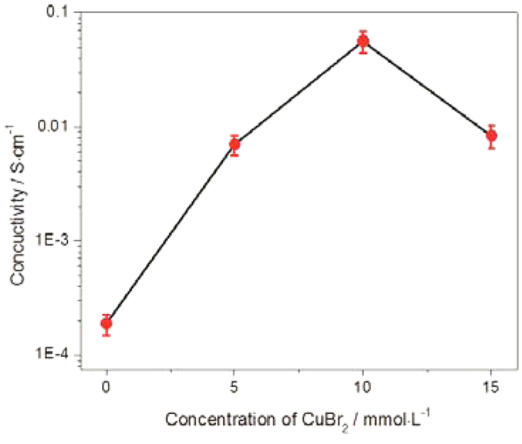

Figure 1. Conductivities of the pristine and $CuBr_2$ doped PEDOT:PSS films with different concentrations of $CuBr_2$ (5−15 mmol·L^{-1}).

conductivity of pristine PEDOT:PSS (Clevios P Al4083) film is 1.9×10^{-4} S·cm^{-1}, which is much lower than that of the reported PEDOT:PSS (Clevios P) film because of the higher weight ratio of PSS to PEDOT and no cosolvent doping in our case.[45,46] Upon $CuBr_2$ doping, a dramatic enhancement of the conductivity of PEDOT:PSS (Clevios P Al4083) film is observed, and the enhancement ratio depends sensitively on the doping concentration of $CuBr_2$. As a result, the conductivity of $CuBr_2$:PEDOT:PSS film reaches 7.0×10^{-3}, 5.6×10^{-2}, and 8.4×10^{-3} S·cm^{-1} under $CuBr_2$ doping concentration of 5, 10, and 15 mmol·L^{-1}, respectively, and the highest conductivity (5.6×10^{-2}) is obtained under the optimized concentration of 10 mmol·L^{-1}, which is improved by about 300 times compared to that of the pristine PEDOT:PSS (Clevios P Al4083) film. However, the enhancement ratio of the conductivity of the PEDOT:PSS film under the optimized $CuBr_2$ doping concentration of 10 mmol·L^{-1} is much lower than that obtained by $CuBr_2$ "dipping" treatment, i.e., dropping the aqueous $CuBr_2$ salt onto the PEDOT:PSS films under heating at 140 °C, as reported in refs 31 and 38. This can be caused by the different composition of PEDOT:PSS (Clevios P Al4083 vs Clevios P) and/or the different conductivity enhancement mechanism of $CuBr_2$ doping to that for $CuBr_2$ "dipping" treatment.[31]

In order to probe whether $CuBr_2$ doping affects the inner composition of the PEDOT:PSS film, we performed X-ray photoelectron spectroscopy (XPS) measurements of PEDOT:PSS films with and without $CuBr_2$ doping. The S(2p) XPS spectra of pristine and $CuBr_2$-doped PEDOT:PSS films are compared in Figure 2. The S(2p) XPS spectrum of the

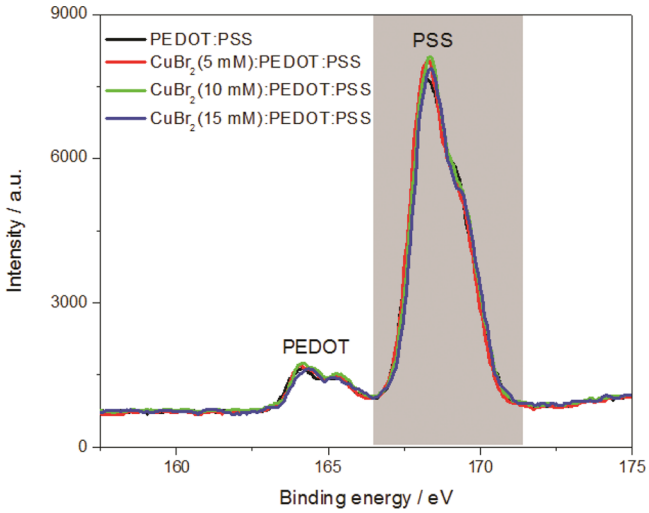

Figure 2. S(2p) XPS spectra of the pristine and $CuBr_2$-doped PEDOT:PSS films with different concentrations of $CuBr_2$ (5−15 mmol·L^{-1}).

pristine PEDOT:PSS film exhibits two signal bands at 162−166 (doublet peaks) and 166−172 eV, which is assigned to the sulfur atoms of PEDOT and PSS, respectively.[29,37] The possible compositional change of the PEDOT and PSS components within PEDOT:PSS film upon $CuBr_2$ doping is probed by the PEDOT-to-PSS ratio calculated according to the integrated peak areas of the S(2p) features of the PEDOT and PSS chains. We found that the PEDOT-to-PSS ratio of $CuBr_2$:PEDOT:PSS film (0.11) keeps constant upon changing $CuBr_2$ doping concentration and is almost the same as that of the pristine PEDOT:PSS film (0.12) (see Supporting Information, Table S1). These results suggest that the composition of the PEDOT:PSS film surface upon $CuBr_2$ doping does not change and a considerable removal of the PSS component from PEDOT:PSS mixture does not take place. Interestingly, this result is dramatically different from the reported case of $CuBr_2$ "dipping" treatment for which a significant PSS loss from the PEDOT:PSS film was observed from XPS characterization contributing partially to the conductivity enhancement of PEDOT:PSS film.[29,31] Such difference can be easily understood because "dipping" post-treatment was not applied to the film in our case. Therefore, the effect of $CuBr_2$ doping on the

DOI: 10.1021/am505387q
ACS Appl. Mater. Interfaces 2015, 7, 1439−1448

conductivity enhancement of PEDOT:PSS film must be different from that obtained by $CuBr_2$ "dipping" treatment as discussed further below.

The transmittance spectra of ITO/$CuBr_2$:PEDOT:PSS film in comparison with that of the ITO/pristine/PEDOT:PSS film are illustrated in Figure 3. The ITO/$CuBr_2$:PEDOT:PSS films

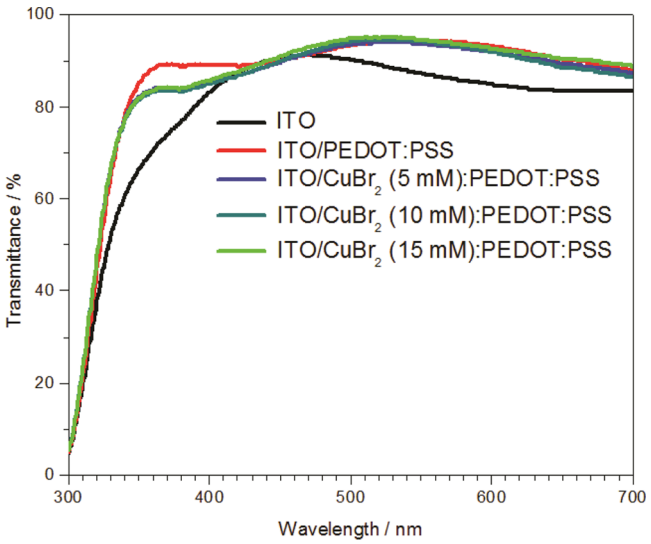

Figure 3. Transmittance spectra of bare ITO, ITO/pristine PEDOT:PSS, and ITO/$CuBr_2$:PEDOT:PSS films with different concentrations of $CuBr_2$.

with 5, 10, and 15 mmol·L^{-1} $CuBr_2$ doping show almost identical transmittance spectra, which are also the same as that of the pristine ITO/PEDOT:PSS film in the wavelength region of 450−700 nm. This feature ensures the applicability of $CuBr_2$:PEDOT:PSS film as HTL in BHJ-PSC, which absorbs light prior to the active layer for the conventional-structure devices. However, the transmittance of ITO/$CuBr_2$:PEDOT:PSS film in the wavelength region of 340−450 nm is lower than that of the pristine ITO/PEDOT:PSS film, and this might result from the absorption of Cu^{2+} ions in this region. Besides, all of the ITO/$CuBr_2$:PEDOT:PSS and pristine ITO/PEDOT:PSS films exhibit higher transmittance in the entire UV−vis region than the bare ITO, and this might be due to the smoother surface upon modification of PEDOT:PSS.[47]

Raman spectroscopy was then employed to probe whether the conformational change of the PEDOT chains within PEDOT:PSS film occurs after $CuBr_2$ doping. As seen in Figure 4, the Raman vibrational band between 1400 and 1500 cm^{-1} corresponding to the stretching vibration of the C═C bonds of PEDOT becomes much stronger in $CuBr_2$:PEDOT:PSS film compared to that in the pristine PEDOT:PSS film, whereas no appreciable shift for the Raman signals is observed. Interestingly, this phenomenon is again different from the reported case of zwitterion "dipping" treatment for which such a Raman vibrational band at 1400−1500 cm^{-1} exhibited a red shift and became narrower owing to the conformational change of some PEDOT chains from benzenoid to quinoid structure after zwitterion "dipping" treatment, which is beneficial for conductivity enhancement of PEDOT:PSS film as well.[29] In our case, the intensity increases of all Raman signals in $CuBr_2$:PEDOT:PSS film are similar to the surface-enhanced Raman scattering (SERS) effect due to the presence of Cu^{2+}

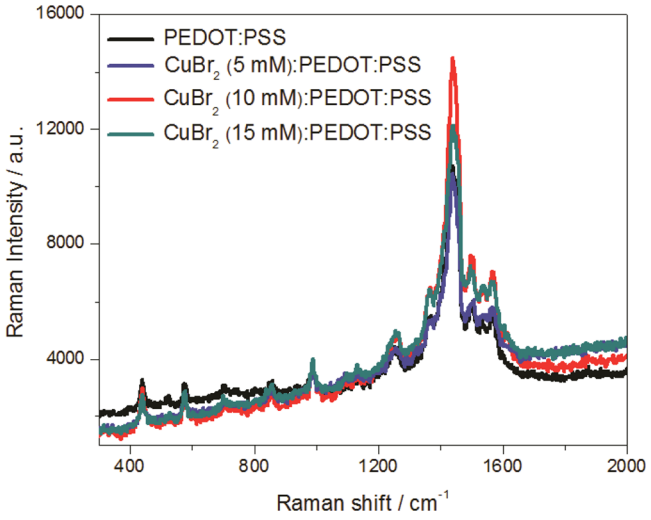

Figure 4. Raman spectra of the pristine and $CuBr_2$-doped PEDOT:PSS films with different concentrations of $CuBr_2$ (5−15 mmol·L^{-1}).

cations.[48] Obviously, $CuBr_2$ (10 mmol·L^{-1}):PEDOT:PSS film exhibits the highest intensity enhancement for the Raman vibrational band between 1400 and 1500 cm^{-1}, suggesting the largest influence of Cu^{2+} cations under this optimum concentration.

On the basis of the above characterizations, a plausible mechanism responsible for the conductivity enhancement of PEDOT:PSS film by $CuBr_2$ doping can be proposed. It is known that within PEDOT:PSS film the PEDOT and PSS chains are entangled by static interactions, leading to positively charged PEDOT and negatively charged PSS chains.[31] When $CuBr_2$ salt dopes PEDOT:PSS, the Cu^{2+} cations may bind to the negatively charged PSS chains while Br^- anions have Coulombic interactions with the positively charged PEDOT chains; thus, $CuBr_2$ doping can effectively screen the charges of PEDOT and PSS moieties. Such a charge screening effect results in weakening of the Coulombic attractions between PEDOT and PSS moieties, facilitating phase separation between the positively charged conducting PEDOT and negatively charged nonconducting PSS chains and consequently contributing to the conductivity enhancement of PEDOT:PSS film. When PEDOT:PSS is overdoped by $CuBr_2$ with a concentration of 15 mmol·L^{-1}, the excess Br^- ions which does not bind to PEDOT chains may prohibit effective stacking of PEDOT chains, resulting in the decrease of conductivity. Nevertheless, since as discussed above $CuBr_2$ doping does not lead to a significant PSS loss from the PEDOT:PSS film reported for the case of $CuBr_2$ "dipping" treatment,[31] the enhancement ratio of the conductivity of PEDOT:PSS film achieved for our case of $CuBr_2$ doping is much lower than that for the reported case of $CuBr_2$ "dipping" treatment.[31] The moderate conductivity enhancement of PEDOT:PSS film upon $CuBr_2$ doping suggests that the influence of Cu^{2+} and Br^- ions in the bulk phase of PEDOT:PSS on the conformations of PEDOT and PSS chains may be more readily controlled than the case of $CuBr_2$ "dipping" treatment, so that the consequent influence of $CuBr_2$ doping on the performance of the BHJ-PSC device can be controlled to avoid deteriorating the performance of the device as discussed in details below.

DOI: 10.1021/am505387q
ACS Appl. Mater. Interfaces 2015, 7, 1439−1448

Performance of PCDTBT:$PC_{71}BM$ BHJ-PSC Devices Based on $CuBr_2$:PEDOT:PSS HTL. Applying $CuBr_2$:PEDOT:PSS as HTL, we fabricated BHJ-PSC devices based on PCDTBT:$PC_{71}BM$ active layer without using any electron transport layer (ETL) so as to simplify the device structure and clarify the influence of HTL solely (see inset of Figure 5). The as-prepared ITO/$CuBr_2$:PEDOT:PSS/PCDTBT:$PC_{71}BM$/Al devices were measured under a simulated AM 1.5 irradiation (100 mW·cm^{-2}) in air atmosphere. The current−voltage (J−V) curves of devices based on $CuBr_2$:PEDOT:PSS HTL with different $CuBr_2$ doping concentrations (denoted as device **C**, **D**, and **E** corresponding to $CuBr_2$ doping concentration of 5, 10, and 15 mmol·L^{-1}, respectively) are compared in Figure 5, which includes those of reference devices without any HTL (device **A**) and with pristine PEDOT:PSS HTL (device **B**) for comparison. The measured parameters including short-circuit current (J_{sc}), open-circuit voltage (V_{oc}), fill factor (FF), PCE, series resistance (R_s), and shunt resistance (R_{sh}) based on the average of more than 10 devices fabricated independently under each experimental condition are summarized in Table 1, and the devices with the highest PCEs were used for the following discussion. The reference device without any HTL (device **A**) shows a relatively low PCE of 4.46% calculated from a V_{oc} of 0.81 V, a J_{sc} of 10.33 mA/cm^2, and a FF of 53.3%. This poor performance may be ascribed to the high work function of ITO (4.7 eV) and the direct contact between ITO and $PC_{71}BM$, leading to a large series resistance and leakage current.[49] When the pristine PEDOT:PSS HTL was incorporated (device **B**), V_{oc}, J_{sc}, and FF all increase to 0.89 V, 11.55 mA/cm^2, and 56.8%, respectively, contributing to the enhanced PCE of 5.84% (Table 1) due to efficient hole transport of PEDOT:PSS.[15] For $CuBr_2$:PEDOT:PSS HTL-incorporated devices (devices **C**−**E**), the PCEs are enhanced obviously compared to that of device **B**, and the enhancement ratio is dependent on the $CuBr_2$ doping concentration. When the $CuBr_2$ doping concentration increases from 5 to 10 mmol·L^{-1}, V_{oc}, J_{sc}, and FF all increase, whereas a further increase of the $CuBr_2$ doping concentration to 15 mmol·L^{-1} results in a dramatic decrease of J_{sc} along with slight decreases of both V_{oc} and FF. Therefore, the optimum $CuBr_2$ doping concentration is determined to be 10 mmol·L^{-1}, under which the highest PCE of 7.05% is achieved and enhanced by ca. 20.7% compared to device **B** (see Table 1 and Supporting Information, Figure S2). To the best of our knowledge, this optimized PCE of 7.05% is the highest one in PCDTBT:$PC_{71}BM$-based BHJ-PSCs without ETL reported so far. Noteworthy, all three photovoltaic parameters of device **D**, V_{oc} (0.95 V), J_{sc} (12.09 mA/cm^2), and FF (61.4%), dramatically increase simultaneously compared to those of devices **A** and **B**, suggesting that $CuBr_2$ doping PEDOT:PSS facilitates hole extraction by ITO anode. Such an efficiency improvement of the device is accomplished by simply doping the commonly used PEDOT:PSS HTL without further "dipping" treatment or spin-coating an additional layer, thus being more facile. In addition, the stability of $CuBr_2$:PEDOT:PSS HTL-based device (device **D**) is obviously improved compared to that of device **B** based on the undoped PEDOT:PSS (see Supporting Information, Figure S3). The effect of $CuBr_2$ doping on photovoltaic performance and stability of PEDOT:PSS HTL-based PSC device is expected to be also applicable for a more conductive PEDOT:PSS such as Clevios P, and this is to be investigated in a follow-up study.

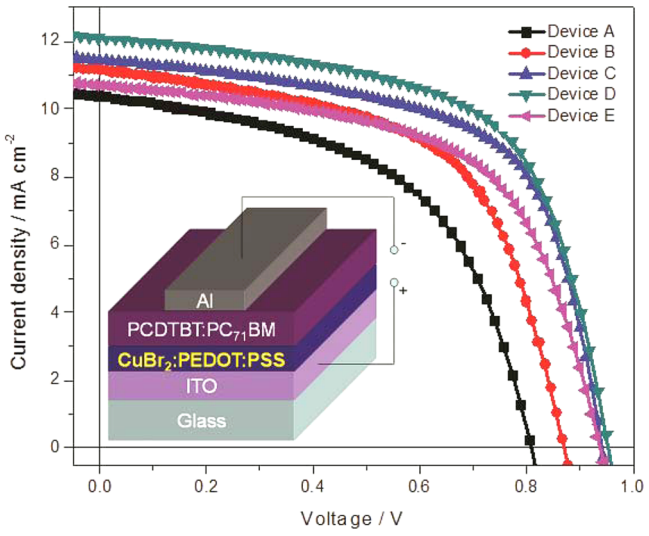

Figure 5. J−V curves of PCDTBT:$PC_{71}BM$ BHJ-PSC devices without any HTL (**A**), with pristine PEDOT:PSS HTL (**B**), and with $CuBr_2$:PEDOT:PSS HTL at different $CuBr_2$ doping concentrations of 5 (**C**), 10 (**D**), and 15 mmol·L^{-1} (**E**). Measurements were carried out under AM 1.5 illumination at an irradiation intensity of 100 mW·cm^{-2}. (Inset) Architecture of the BHJ-PSC device.

The dependence of the enhancement ratio of each photovoltaic parameter determining PCE (including V_{oc}, J_{sc}, and FF) on the HTL was plotted so as to unveil the factors responsible for the enhanced PCE upon $CuBr_2$ doping PEDOT:PSS (see Supporting Information, Figure S2). Clearly, the enhanced PCE based on $CuBr_2$:PEDOT:PSS HTL compared to that based on pristine PEDOT:PSS HTL is mainly resulted from the 6.7% and 8.1% enhancements of V_{oc} and FF for device **D**, respectively. It is generally known that the

Table 1. Photovoltaic Parameters of the ITO/$CuBr_2$:PEDOT:PSS/PCDTBT:$PC_{71}BM$/Al BHJ-PSC Devices with Different HTLs

					PCE (%)			
device	[$CuBr_2$][a] (mmol·L^{-1})	V_{oc} (V)	J_{sc} (mA/cm^2)	FF (%)	highest	average[b]	R_s[c] (Ω·cm^2)	R_{sh}[c] (Ω·cm^2)
A	*d*	0.81	10.33	53.3	4.46	4.40 ± 0.06	19.4	435.1
B	0	0.89	11.55	56.8	5.84	5.65 ± 0.12	17.0	553.9
C	5	0.94	11.65	61.0	6.68	6.53 ± 0.11	13.0	696.3
D	10	0.95	12.09	61.4	7.05	6.97 ± 0.05	10.9	720.3
E	15	0.93	10.63	60.9	6.02	5.96 ± 0.05	14.6	656.6

[a]$CuBr_2$ doping concentration in PEDOT:PSS HTL. [b]Averaged over ten devices. [c]R_s and R_{sh} are given by the PCE measurement system. [d]Without any HTL.

DOI: 10.1021/am505387q
ACS Appl. Mater. Interfaces 2015, 7, 1439−1448

maximum attainable V_{oc} is primarily correlated to the difference between the donor HOMO level and the acceptor LUMO level, and the actual V_{oc} is also affected by the work functions of the electrodes and the interfacial layer materials.[50,51] In our case, since the electrodes and donor:acceptor active layer are the same when changing the HTL in devices **B**–**E**, the difference in V_{oc} must be due to the variation of the work function of PEDOT:PSS HTL.[50] Since there is an energy level barrier (0.8 eV) between the work function of ITO (4.7 eV) and the HOMO level of the PCDTBT donor (5.5 eV) (Scheme 1),[43] an unfavorable hole extraction occurs, resulting in poor

Scheme 1. Energy Level Diagram of ITO/$CuBr_2$:PEDOT:PSS/PCDTBT:$PC_{71}BM$/Al BHJ-PSC Devices with Pristine and $CuBr_2$-Doped PEDOT:PSS HTL[a]

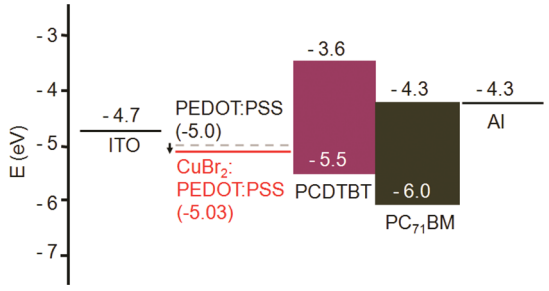

[a]HOMO/LUMO levels of PCDTBT and $PC_{71}BM$ and the work functions of ITO, pristine PEDOT:PSS, and Al were referred to ref 43.

performance of device **A** without any HTL.[50] Upon incorporation of the pristine PEDOT:PSS HTL with an intermediate work function of 5.0 eV (device **B**),[43] the increase of V_{oc} compared to that of the reference device **A** is interpreted by the formation of an Ohmic contact between ITO/PCDTBT interface avoiding such an energy barrier as reported in the literature for BHJ-PSC devices based on different active layers.[15,52] When $CuBr_2$:PEDOT:PSS HTL was used (devices **C**–**E**), the increase of V_{oc} relative to that of device **B** is expected to result from the variation of the work function of PEDOT:PSS HTL, which is experimentally confirmed as discussed further below. On the other hand, FF is determined by charge carriers reaching the electrodes, when the built-in field is lowered toward the open circuit voltage, and is more sensitive than V_{oc} and J_{sc} to the electrode/active layer interface.[15,37,53,54] Thus, the increase of FF for devices **C**–**E** compared to that of device **B** should be attributed to the improved ITO/PCDTBT interface as a result of the varied work function of PEDOT:PSS HTL, facilitating hole extraction.

Surface Morphologies of $CuBr_2$:PEDOT:PSS HTL and PCDTBT:$PC_{71}BM$ Films. In order to figure out the morphological influence of $CuBr_2$ doping on PEDOT:PSS HTL and PCDTBT:$PC_{71}BM$ active layer films, we measured the surface morphologies of PEDOT:PSS HTL and PCDTBT:$PC_{71}BM$ films by atomic force microscopy (AFM) in tapping mode (Figure 6). As seen from the AFM height image of $CuBr_2$:PEDOT:PSS film corresponding to device **D** ($CuBr_2$ doping concentration at 10 mmol·L^{-1}) in comparison with that of the pristine PEDOT:PSS film within device **B**, both pristine (image a) and $CuBr_2$-doped PEDOT:PSS film (image b) have quite smooth surfaces (see Supporting Information, Figure S4(a) and S4(b) for 3D AFM images), while the surface of the latter one is smoother than that of the former as indicated by the decrease of the root-mean-square (RMS)

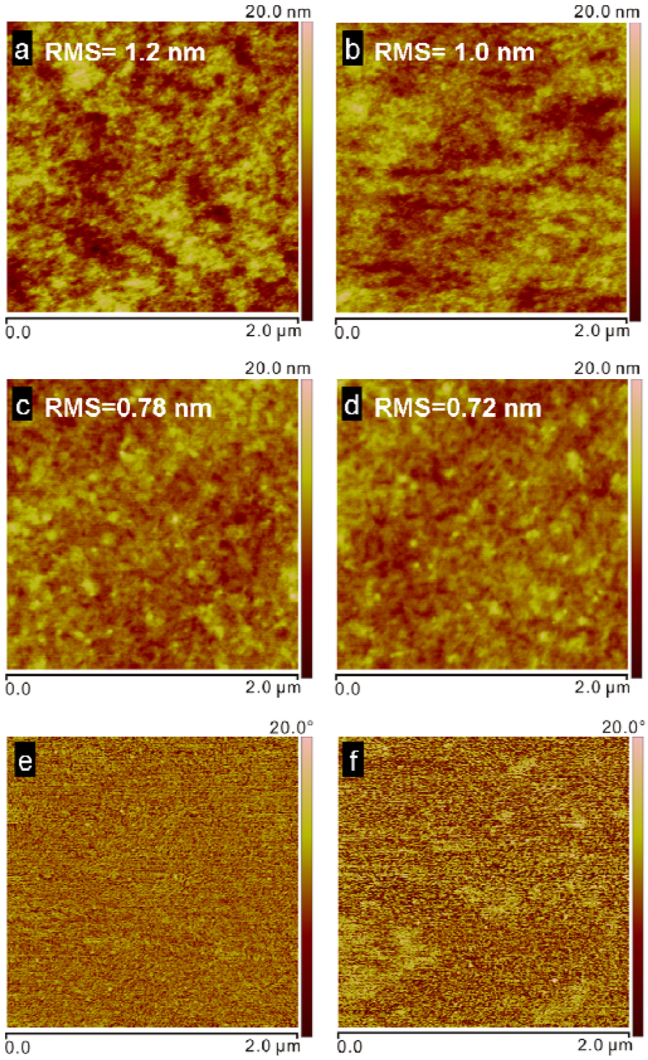

Figure 6. AFM height images of pristine PEDOT:PSS (a), $CuBr_2$ (10 mmol·L^{-1}):PEDOT:PSS (b), pristine PEDOT:PSS/PCDTBT:$PC_{71}BM$ (c), and $CuBr_2$ (10 mmol·L^{-1}):PEDOT:PSS/PCDTBT:$PC_{71}BM$ films (d). Corresponding AFM phase images of pristine PEDOT:PSS/PCDTBT:$PC_{71}BM$ (e) and $CuBr_2$ (10 mmol·L^{-1}):PEDOT:PSS/PCDTBT:$PC_{71}BM$ films (f) are also shown.

roughness from 1.2 to 1.0 nm. Interestingly, this result is contrary to that reported for PEDOT:PSS film with $CuBr_2$ "dipping" treatment, for which the RMS roughness of PEDOT:PSS film treated by $CuBr_2$ ($CuSO_4$, InI_3) dramatically increased compared to that of the pristine film due to the increased grain size as a result of the PSS loss from the PEDOT:PSS film.[31] Obviously, such a great discrepancy between our doping treatment and the reported "dipping" treatment is owing to the different influence mechanism of $CuBr_2$ salt on PEDOT:PSS film as discussed above.

AFM images of PCDTBT:$PC_{71}BM$ active layer films fabricated on pristine and $CuBr_2$ (10 mmol·L^{-1}) doped PEDOT:PSS films are illustrated in Figure 6 in both height and phase modes (Figure 6c–f). According to the AFM height images (Figure 6c and 6d), the RMS roughnesses of the PEDOT:PSS/PCDTBT:$PC_{71}BM$ and $CuBr_2$:PEDOT:PSS/PCDTBT:$PC_{71}BM$ films are quite comparable (0.78 vs 0.72 nm). However, as seen from their AFM phase images in which the bright and dark regions correspond to the PCDTBT donor and the $PC_{71}BM$ acceptor phases, respectively, the contrast

DOI: 10.1021/am505387q
ACS Appl. Mater. Interfaces 2015, 7, 1439–1448

between the bright and the dark regions for $CuBr_2$:PEDOT:PSS/PCDTBT:$PC_{71}BM$ film (Figure 6f) is obviously higher than that for PEDOT:PSS/PCDTBT:$PC_{71}BM$ film (Figure 6e). In previous reports the enhanced contrast was generally attributed to the increased phase separation between donor and acceptor phases in BHJ-PSC devices.[53,55] Therefore, these results suggest that in addition to the influence on PEDOT:PSS HTL film itself $CuBr_2$ doping further improves the phase separation within the PCDTBT:$PC_{71}BM$ active layer film, and this effect should be partially responsible for the enhanced device performance upon incorporation of $CuBr_2$:PEDOT:PSS HTL.

Mechanism of the Efficiency Enhancement of PCDTBT:$PC_{71}BM$ BHJ-PSC Devices Upon $CuBr_2$ Doping. As discussed above, the efficiency enhancement of PCDTBT:$PC_{71}BM$ BHJ-PSC devices based on $CuBr_2$:PEDOT:PSS HTL is mainly due to the synergetic increases of both V_{oc} and FF. In order to confirm that the increase of V_{oc} of device based on $CuBr_2$:PEDOT:PSS HTL is resulted from the variation of the work function of PEDOT:PSS HTL, we carried out scanning Kelvin probe microscopy (SKPM) measurements, which can directly probe the interfacial dipole induced by interfacial layer and can be further used to estimate the work function of interfacial material.[11,18,56−58] On the basis of the detailed analysis of the surface potential value, we found that the surface potential of $CuBr_2$:PEDOT:PSS HTL is ca. 30 mV more positive than that of the undoped PEDOT:PSS HTL (see Supporting Information, Figure S5 and Table S2). Assuming that the surface potential of the pristine or $CuBr_2$-doped PEDOT:PSS film is uniform in macroscopic scale, the change of the surface potential value upon $CuBr_2$ doping can be directly correlated to the change of the work function of the $CuBr_2$:PEDOT:PSS HTL.[11,18,56−58] Thus, the work function of the $CuBr_2$ (10 mmol·L^{-1}):PEDOT:PSS HTL is estimated to increase by ca. 30 meV relative to that of the pristine PEDOT:PSS HTL, which was reported to be 5.0 eV.[5,43] With such an increase of the work function of PEDOT:PSS HTL upon $CuBr_2$ doping, the work function of the $CuBr_2$:PEDOT:PSS HTL becomes more close to the HOMO level of the PCDTBT donor (5.5 eV) (see Scheme 1) and consequently benefiting an Ohmic contact formation between ITO/PCDTBT interface.

Increasing the work function of PEDOT:PSS has been realized by physical treatment such as UV light irradiation.[59] The enhanced efficiency is mainly attributed to the increase of J_{sc}, and these phenomena are essentially different to our case of doping aqueous PEDOT:PSS solution by $CuBr_2$ salt, suggesting the peculiarity of the efficiency enhancement mechanism for $CuBr_2$ doping. On the other hand, the work function of PEDOT:PSS can be also tuned by chemical treatment via doping with high boiling point solvents such as dimethyl sulfoxide (DMSO), sorbitol, glycerol, etc., but such treatments generally lead to a decrease of the work function of PEDOT:PSS.[19,60,61]

It has been revealed in the literature that the content of the negatively charged PSS moiety (PSS^-) within the PEDOT:PSS film plays an important role in the work function of the PEDOT:PSS film.[62] In our case, although $CuBr_2$ doping had not led to the PSS loss from the PEDOT:PSS film surface, the introduced Br^- may behave as the charge compensating counterions of $PEDOT^+$, resulting in the weakening of the Coulombic attractions between PSS and PEDOT chains and contributing to an increased work function. Besides, given that the optimized $CuBr_2$ doping concentration (10 mmol·L^{-1}) for the highest PCE is the same as that optimized for the conductivity of $CuBr_2$:PEDOT:PSS film as discussed above, it is reasonable to attribute the improved conductivity of PEDOT:PSS film upon $CuBr_2$ doping as an conjunct reason to the improved PCE of devices based on $CuBr_2$:PEDOT:PSS HTL. However, the improved conductivity of PEDOT:PSS film by polar solvent doping generally leads to the obvious increase of J_{sc} in the literature.[34] This is quite different to our case of $CuBr_2$ doping, for which a slight increase of J_{sc} (much lower than that of V_{oc}) is observed only at a relatively low $CuBr_2$ doping concentration (devices **C** and **D**), whereas J_{sc} decreases instead for device **E** with high $CuBr_2$ doping concentration (see Table 1 and Figure S2, Supporting Information). A plausible interpretation is that the lower transmittance of $CuBr_2$:PEDOT:PSS film than that of the pristine PEDOT:PSS film in the wavelength region of 340−450 nm led to less light absorption of the PCDTBT:$PC_{71}BM$ active layer (see Figure 3), and this offsets the increase of J_{sc} by the enhanced conductivity upon $CuBr_2$ doping.

The proposed electrostatic model accounting for the efficiency enhancement of PCDTBT:$PC_{71}BM$ BHJ-PSC devices via $CuBr_2$ doping is further confirmed experimentally by applying other Cu^{2+} salts with different halogen anions such as $CuCl_2$ and CuI_2 as dopant of PEDOT:PSS. According to our preliminary results, under the same doping concentration of 10 mmol·L^{-1} and identical device fabrication conditions, PCDTBT:$PC_{71}BM$ BHJ-PSC devices based on $CuCl_2$- or CuI_2-doped PEDOT:PSS HTL exhibit PCE of 6.11% and 4.28%, respectively (see Supporting Information, Figure S6 and Table S3), which are both much lower than that based on the $CuBr_2$-doped one. Despite the fact that the $CuCl_2$:PEDOT:PSS HTL-based device shows an enhanced PCE relative to that based on pristine PEDOT:PSS HTL, its PCE is obviously lower than that of the $CuBr_2$:PEDOT:PSS HTL-based device; this can be explained by the lower conductivity enhancement of $CuCl_2$:PEDOT:PSS because of the smaller softness parameter of Cl^- anion as revealed in the literature.[31] On the other hand, because CuI_2 is barely soluble in aqueous PEDOT:PSS solution, CuI_2 doping in PEDOT:PSS HTL led to a dramatic decrease on PCE, which is even lower than that of the reference device based on pristine PEDOT:PSS HTL, revealing that CuI_2 doping deteriorates the performance of PSC device. A systematic study to unveil further the dependence of metal cation and anion on the performance of salt doping is underway in our lab.

The increase of FF in $CuBr_2$:PEDOT:PSS HTL-based device compared to that based on pristine PEDOT:PSS HTL is consistent with the changes of R_s and R_{sh}: when FF increases from 56.8% (device **B**) to 61.4% (device **D**), R_s decreases from 17.0 to 10.9 Ω·cm^2 along with an obvious increase of R_{sh} (Table 1).[63] These results suggest that, benefited from the increased work function of PEDOT:PSS HTL by $CuBr_2$ doping, the Ohmic contact between the ITO/PCDTBT interface is improved to facilitate hole extraction by the ITO anode with the leakage current suppressed.

CONCLUSIONS

In summary, PEDOT:PSS was doped by $CuBr_2$ and used as HTL of PCDTBT:$PC_{71}BM$ BHJ-PSC devices, resulting in dramatically improved conductivity of PEDOT:PSS HTL and consequently improved PCE of the device. Under the optimized doping concentration of $CuBr_2$ of 10 mmol·L^{-1},

DOI: 10.1021/am505387q
ACS Appl. Mater. Interfaces 2015, 7, 1439−1448

PCE of the $CuBr_2$:PEDOT:PSS HTL-incorporated PCDTBT:$PC_{71}BM$ BHJ-PSC device reaches 7.05%, which is improved by ~20.7% compared to that of the reference device based on pristine PEDOT:PSS HTL and represents the highest PCE for PCDTBT:$PC_{71}BM$-based BHJ-PSC devices without ETL reported so far. The improved PCE is mainly due to the increase of both V_{oc} and FF. The increase of V_{oc} of a device based on $CuBr_2$:PEDOT:PSS HTL compared to that based on pristine PEDOT:PSS HTL results from the increase of the work function of PEDOT:PSS by 30 meV as inferred from SKPM measurements. The improved conductivity of PEDOT:PSS film by $CuBr_2$ doping is also proposed as an conjunct reason responsible for the improved PCE of devices based on $CuBr_2$:PEDOT:PSS HTL. The increased work function of PEDOT:PSS HTL by $CuBr_2$ doping contributes to the improved ITO/PCDTBT interface as well, facilitating hole extraction by the ITO anode and leading to the increase of FF. Our method toward improving performance of BHJ-PSC device is accomplished by simply doping the commonly used PEDOT:PSS HTL without further "dipping" treatment or spin-coating an additional layer, providing a facile route for enhancing the performance of PSCs.

■ ASSOCIATED CONTENT

Supporting Information

Determination of the thickness of $CuBr_2$-doped PEDOT:PSS HTL by profilometer, determination of the PEDOT-to-PSS ratio by S(2p) XPS results, enhancement ratio of each photovoltaic parameter, 3D AFM images of pristine and $CuBr_2$ (10 $mmol \cdot L^{-1}$) doped PEDOT:PSS HTL and PCDTBT:$PC_{71}BM$ films, determination of work function of PEDOT:PSS HTLs by SKPM, performance of PCDTBT:$PC_{71}BM$ BHJ-PSC devices based on PEDOT:PSS HTL doped by different copper(II) halides, etc. This material is available free of charge via the Internet at http://pubs.acs.org.

■ AUTHOR INFORMATION

Corresponding Author

*E-mail: sfyang@ustc.edu.cn.

Notes

The authors declare no competing financial interest.

■ ACKNOWLEDGMENTS

This work was partially supported by National Natural Science Foundation of China (Nos. 21132007, 21371164), Key Project of Hefei Center for Physical Science and Technology (No. 2012FXZY006), and National Basic Research Program of China (2010CB923300, 2011CB921400).

■ REFERENCES

(1) Yu, G.; Gao, J.; Hummelen, J. C.; Wudl, F.; Heeger, A. J. Polymer Photovoltaic Cells - Enhanced Efficiencies Via a Network of Internal Donor-Acceptor Heterojunctions. *Science* **1995**, *270*, 1789−1791.

(2) Gunes, S.; Neugebauer, H.; Sariciftci, N. S. Conjugated Polymer-Based Organic Solar Cells. *Chem. Rev.* **2007**, *107*, 1324−1338.

(3) He, Z. C.; Zhong, C. M.; Su, S. J.; Xu, M.; Wu, H. B.; Cao, Y. Enhanced Power-Conversion Efficiency in Polymer Solar Cells Using an Inverted Device Structure. *Nat. Photonics* **2012**, *6*, 591−595.

(4) He, Z.; Wu, H.; Cao, Y. Recent Advances in Polymer Solar Cells: Realization of High Device Performance by Incorporating Water/Alcohol-Soluble Conjugated Polymers as Electrode Buffer Layer. *Adv. Mater.* **2014**, *26*, 1006−1024.

(5) Li, G.; Zhu, R.; Yang, Y. Polymer Solar Cells. *Nat. Photonics* **2012**, *6*, 153−161.

(6) Krebs, F. C.; Jorgensen, M. 2D Characterization of OPV from Single and Tandem Cells to Fully Roll-to-Roll Processed Modules with and without Electrical Contact. *Adv. Opt. Mater.* **2014**, *2*, 465−477.

(7) Carle, J. E.; Helgesen, M.; Madsen, M. V.; Bundgaard, E.; Krebs, F. C. Upscaling from Single Cells to Modules - Fabrication of Vacuum- and ITO-Free Polymer Solar Cells on Flexible Substrates with Long Lifetime. *J. Mater. Chem. C* **2014**, *2*, 1290−1297.

(8) You, J. B.; Dou, L. T.; Yoshimura, K.; Kato, T.; Ohya, K.; Moriarty, T.; Emery, K.; Chen, C. C.; Gao, J.; Li, G.; Yang, Y. A Polymer Tandem Solar Cell with 10.6% Power Conversion Efficiency. *Nat. Commun.* **2013**, *4*, 1446.

(9) You, J. B.; Chen, C. C.; Hong, Z. R.; Yoshimura, K.; Ohya, K.; Xu, R.; Ye, S. L.; Gao, J.; Li, G.; Yang, Y. 10.2% Power Conversion Efficiency Polymer Tandem Solar Cells Consisting of Two Identical Sub-Cells. *Adv. Mater.* **2013**, *25*, 3973−3978.

(10) Guo, X. G.; Zhou, N. J.; Lou, S. J.; Smith, J.; Tice, D. B.; Hennek, J. W.; Ortiz, R. P.; Navarrete, J. T. L.; Li, S. Y.; Strzalka, J.; Chen, L. X.; Chang, R. P. H.; Facchetti, A.; Marks, T. J. Polymer Solar Cells with Enhanced Fill Factors. *Nat. Photonics* **2013**, *7*, 825−833.

(11) Zhao, X. M.; Xu, C. H.; Wang, H. T.; Chen, F.; Zhang, W. F.; Zhao, Z. Q.; Chen, L. W.; Yang, S. F. Application of Biuret, Dicyandiamide, or Urea as a Cathode Buffer Layer toward the Efficiency Enhancement of Polymer Solar Cells. *ACS Appl. Mater. Interfaces* **2014**, *6*, 4329−4337.

(12) Liao, S. H.; Jhuo, H. J.; Cheng, Y. S.; Chen, S. A. Fullerene Derivative-Doped Zinc Oxide Nanofilm as the Cathode of Inverted Polymer Solar Cells with Low-Bandgap Polymer (PTB7-Th) for High Performance. *Adv. Mater.* **2013**, *25*, 4766−4771.

(13) Moule, A. J.; Meerholz, K. Controlling Morphology in Polymer-Fullerene Mixtures. *Adv. Mater.* **2008**, *20*, 240.

(14) Zhang, F. L.; Jespersen, K. G.; Bjorstrom, C.; Svensson, M.; Andersson, M. R.; Sundstrom, V.; Magnusson, K.; Moons, E.; Yartsev, A.; Inganas, O. Influence of Solvent Mixing on the Morphology and Performance of Solar Cells Based on Polyfluorene Copolymer/Fullerene Blends. *Adv. Funct. Mater.* **2006**, *16*, 667−674.

(15) Po, R.; Carbonera, C.; Bernardi, A.; Camaioni, N. The Role of Buffer Layers in Polymer Solar Cells. *Energy Environ. Sci.* **2011**, *4*, 285−310.

(16) Chen, S.; Manders, J. R.; Tsang, S.-W.; So, F. Metal Oxides for Interface Engineering in Polymer Solar Cells. *J. Mater. Chem.* **2012**, *22*, 24202−24212.

(17) Ma, H.; Yip, H. L.; Huang, F.; Jen, A. K. Y. Interface Engineering for Organic Electronics. *Adv. Funct. Mater.* **2010**, *20*, 1371−1388.

(18) Qu, S. X.; Li, M. H.; Xie, L. X.; Huang, X.; Yang, J. G.; Wang, N.; Yang, S. F. Noncovalent Functionalization of Graphene Attaching 6,6 -Phenyl-C61-butyric Acid Methyl Ester (PCBM) and Application as Electron Extraction Layer of Polymer Solar Cells. *ACS Nano* **2013**, *7*, 4070−4081.

(19) Nardes, A. M.; Kemerink, M.; de Kok, M. M.; Vinken, E.; Maturova, K.; Janssen, R. A. J. Conductivity, Work Function, and Environmental Stability of PEDOT: PSS Thin Films Treated with Sorbitol. *Org. Electron.* **2008**, *9*, 727−734.

(20) Kim, Y. H.; Sachse, C.; Machala, M. L.; May, C.; Muller-Meskamp, L.; Leo, K. Highly Conductive PEDOT:PSS Electrode with Optimized Solvent and Thermal Post-Treatment for ITO-Free Organic Solar Cells. *Adv. Funct. Mater.* **2011**, *21*, 1076−1081.

(21) Hao, Z. H.; Hu, Z. Y.; Zhang, J. J.; Hao, Q. Y.; Zhao, Y. Influence of Doped PEDOT: PSS on Performance of Polymer Solar Cells. *Acta. Phys. Sin.* **2011**, *60*, 117106.

(22) Xie, F. X.; Choy, W. C. H.; Wang, C. D.; Li, X. C.; Zhang, S. Q.; Hou, J. H. Low-Temperature Solution-Processed Hydrogen Molybdenum and Vanadium Bronzes for an Efficient Hole-Transport Layer in Organic Electronics. *Adv. Mater.* **2013**, *25*, 2051−2055.

DOI: 10.1021/am505387q
ACS Appl. Mater. Interfaces 2015, 7, 1439−1448

(23) Zilberberg, K.; Gharbi, H.; Behrendt, A.; Trost, S.; Riedl, T. Low-Temperature, Solution-Processed MoOx for Efficient and Stable Organic Solar Cells. *ACS Appl. Mater. Interfaces* **2012**, *4*, 1164−1168.
(24) Lim, T. H.; Oh, K. W.; Kim, S. H. Self-Assembly Supramolecules to Enhance Electrical Conductivity of Polyaniline for a Flexible Organic Solar Cells Anode. *Sol. Energy Mater. Sol. Cells* **2012**, *101*, 232−240.
(25) Lu, K. Y.; Yuan, J. Y.; Peng, J.; Huang, X. D.; Cui, L. S.; Jiang, Z. Q.; Wang, H. Q.; Ma, W. L. New Solution-Processable Small Molecules as Hole-Transporting Layer in Efficient Polymer Solar Cells. *J. Mater. Chem. A* **2013**, *1*, 14253−14261.
(26) Li, S.-S.; Tu, K.-H.; Lin, C.-C.; Chen, C.-W.; Chhowalla, M. Solution-Processable Graphene Oxide as an Efficient Hole Transport Layer in Polymer Solar Cells. *ACS Nano* **2010**, *4*, 3169−3174.
(27) Chao, Y. H.; Wu, J. S.; Wu, C. E.; Jheng, J. F.; Wang, C. L.; Hsu, C. S. Solution-Processed (Graphene Oxide)-(d(0) Transition Metal Oxide) Composite Anodic Buffer Layers toward High-Performance and Durable Inverted Polymer Solar Cells. *Adv. Energy Mater.* **2013**, *3*, 1279−1285.
(28) Groenendaal, B. L.; Jonas, F.; Freitag, D.; Pielartzik, H.; Reynolds, J. R. Poly(3,4-ethylenedioxythiophene) and its Derivatives: Past, Present, and Future. *Adv. Mater.* **2000**, *12*, 481−494.
(29) Xia, Y. J.; Zhang, H. M.; Ouyang, J. Y. Highly Conductive PEDOT:PSS Films Prepared Through a Treatment with Zwitterions and Their Application in Polymer Photovoltaic Cells. *J. Mater. Chem.* **2010**, *20*, 9740−9747.
(30) Nagata, T.; Oha, S.; Chikyow, T.; Wakayama, Y. Effect of UV-Ozone Treatment on Electrical Properties of PEDOT:PSS Film. *Org. Electron.* **2011**, *12*, 279−284.
(31) Xia, Y. J.; Ouyang, J. Y. Anion Effect on Salt-Induced Conductivity Enhancement of Poly(3,4-ethylenedioxythiophene):Poly(styrenesulfonate) Films. *Org. Electron.* **2010**, *11*, 1129−1135.
(32) Aernouts, T.; Geens, W.; Poortmans, J.; Heremans, P.; Borghs, S.; Mertens, R. Extraction of Bulk and Contact Components of the Series Resistance in Organic Bulk Donor-Acceptor-Heterojunctions. *Thin Solid Films* **2002**, *403*, 297−301.
(33) Hu, Z. Y.; Zhang, J. J.; Hao, Z. H.; Zhao, Y. Influence of Doped PEDOT:PSS on the Performance of Polymer Solar Cells. *Sol. Energy Mater. Sol. Cells* **2011**, *95*, 2763−2767.
(34) Yang, J. S.; Oh, S. H.; Kim, D. L.; Kim, S. J.; Kim, H. J. Hole Transport Enhancing Effects of Polar Solvents on Poly(3,4-ethylenedioxythiophene):Poly(styrene sulfonic acid) for Organic Solar Cells. *ACS Appl. Mater. Interfaces* **2012**, *4*, 5394−5398.
(35) Dimitriev, O. P.; Grinko, D. A.; Noskov, Y. V.; Ogurtsov, N. A.; Pud, A. A. PEDOT:PSS Films-Effect of Organic Solvent Additives and Annealing on the Film Conductivity. *Synth. Met.* **2009**, *159*, 2237−2239.
(36) Dobbelin, M.; Marcilla, R.; Salsamendi, M.; Pozo-Gonzalo, C.; Carrasco, P. M.; Pomposo, J. A.; Mecerreyes, D. Influence of Ionic Liquids on the Electrical Conductivity and Morphology of PEDOT:PSS Films. *Chem. Mater.* **2007**, *19*, 2147−2149.
(37) Zhang, W. F.; Zhao, B. F.; He, Z. C.; Zhao, X. M.; Wang, H. T.; Yang, S. F.; Wu, H. B.; Cao, Y. High-Efficiency ITO-Free Polymer Solar Cells Using Highly Conductive PEDOT:PSS/Surfactant Bilayer Transparent Anodes. *Energy Environ. Sci.* **2013**, *6*, 1956−1964.
(38) Xia, Y. J.; Ouyang, J. Y. Salt-Induced Charge Screening and Significant Conductivity Enhancement of Conducting Poly(3,4-ethylenedioxythiophene):Poly(styrenesulfonate). *Macromolecules* **2009**, *42*, 4141−4147.
(39) Xia, Y. J.; Sun, K.; Ouyang, J. Y. Solution-Processed Metallic Conducting Polymer Films as Transparent Electrode of Optoelectronic Devices. *Adv. Mater.* **2012**, *24*, 2436−2440.
(40) Chen, B. X.; Zhang, W. F.; Zhou, X. H.; Huang, X.; Zhao, X. M.; Wang, H. T.; Liu, M.; Lu, Y. L.; Yang, S. F. Surface Plasmon Enhancement of Polymer Solar Cells by Penetrating Au/SiO2 Core/Shell Nanoparticles into all Organic Layers. *Nano Energy* **2013**, *2*, 906−915.
(41) Wang, H. T.; Zhang, W. F.; Xu, C. H.; Bi, X. H.; Chen, B. X.; Yang, S. F. Efficiency Enhancement of Polymer Solar Cells by Applying Poly(vinylpyrrolidone) as a Cathode Buffer Layer via Spin Coating or Self-Assembly. *ACS Appl. Mater. Interfaces* **2013**, *5*, 26−34.
(42) Zhang, W. F.; Wang, H. T.; Chen, B. X.; Bi, X. H.; Venkatesan, S.; Qiao, Q. Q.; Yang, S. F. Oleamide as a Self-Assembled Cathode Buffer Layer for Polymer Solar Cells: the Role of the Terminal Group on the Gunction of the Surfactant. *J. Mater. Chem.* **2012**, *22*, 24067−24074.
(43) Park, S. H.; Roy, A.; Beaupre, S.; Cho, S.; Coates, N.; Moon, J. S.; Moses, D.; Leclerc, M.; Lee, K.; Heeger, A. J. Bulk Heterojunction Solar Cells with Internal Quantum Efficiency Approaching 100%. *Nat. Photonics* **2009**, *3*, 297.
(44) Snaith, H. J. How should you measure your excitonic solar cells? *Energy Environ. Sci.* **2012**, *5*, 6513−6520.
(45) Nardes, A. M.; Kemerink, M.; Janssen, R. A. J.; Bastiaansen, J. A. M.; Kiggen, N. M. M.; Langeveld, B. M. W.; van Breemen, A. J. J. M.; de Kok, M. M. Microscopic Understanding of the Anisotropic Conductivity of PEDOT: PSS Thin Films. *Adv. Mater.* **2007**, *19*, 1196.
(46) Palumbiny, C. M.; Heller, C.; Schaffer, C. J.; Körstgens, V.; Santoro, G.; Roth, S. V.; Müller-Buschbaum, P. Molecular Reorientation and Structural Changes in Cosolvent-Treated Highly Conductive PEDOT:PSS Electrodes for Flexible Indium Tin Oxide-Free Organic Electronics. *J. Phys. Chem. C* **2014**, *118*, 13598−13606.
(47) Sun, Y. M.; Seo, J. H.; Takacs, C. J.; Seifter, J.; Heeger, A. J. Inverted Polymer Solar Cells Integrated with a Low-Temperature-Annealed Sol-Gel-Derived ZnO Film as an Electron Transport Layer. *Adv. Mater.* **2011**, *23*, 1679.
(48) Yan, X.; Zhang, X. J.; Yuan, Y. X.; Han, S. Y.; Xu, M. M.; Gu, R.; Yao, J. L. Magnetic Separation of Heavy Metal Ions and Evaluation Based on Surface-Enhanced Raman Spectroscopy: Copper(II) Ions as a Case Study. *J. Sep. Sci.* **2013**, *36*, 3651−3657.
(49) Li, X. D.; Zhang, W. J.; Wu, Y. L.; Min, C.; Fang, J. F. Solution-Processed MoSx as an Efficient Anode Buffer Layer in Organic Solar Cells. *ACS Appl. Mater. Interfaces* **2013**, *5*, 8823−8827.
(50) Ratcliff, E. L.; Garcia, A.; Paniagua, S. A.; Cowan, S. R.; Giordano, A. J.; Ginley, D. S.; Marder, S. R.; Berry, J. J.; Olson, D. C. Investigating the Influence of Interfacial Contact Properties on Open Circuit Voltages in Organic Photovoltaic Performance: Work Function Versus Selectivity. *Adv. Energy Mater.* **2013**, *3*, 647−656.
(51) Wagenpfahl, A.; Rauh, D.; Binder, M.; Deibel, C.; Dyakonov, V. S-shaped Current-Voltage Characteristics of Organic Solar Devices. *Phys. Rev. B* **2010**, *82*, 115306.
(52) Xu, Q.; Wang, F. Z.; Tan, Z. A.; Li, L. J.; Li, S. S.; Hou, X. L.; Sun, G.; Tu, X. H.; Hou, J. H.; Li, Y. F. High-Performance Polymer Solar Cells with Solution-Processed and Environmentally Friendly CuOx Anode Buffer Layer. *ACS Appl. Mater. Interfaces* **2013**, *5*, 10658−10664.
(53) Di Nuzzo, D.; Aguirre, A.; Shahid, M.; Gevaerts, V. S.; Meskers, S. C. J.; Janssen, R. A. J. Improved Film Morphology Reduces Charge Carrier Recombination into the Triplet Excited State in a Small Bandgap Polymer-Fullerene Photovoltaic Cell. *Adv. Mater.* **2010**, *22*, 4321.
(54) Zhang, W. F.; Xu, Y.; Wang, H. T.; Xu, C. H.; Yang, S. F. Fe3O4 Nanoparticles Induced Magnetic Field Effect on Efficiency Enhancement of P3HT:PCBM Bulk Heterojunction Polymer Solar Cells. *Sol. Energy Mater. Sol Cells* **2011**, *95*, 2880−2885.
(55) Chu, T. Y.; Alem, S.; Tsang, S. W.; Tse, S. C.; Wakim, S.; Lu, J. P.; Dennler, G.; Waller, D.; Gaudiana, R.; Tao, Y. Morphology Control in Polycarbazole Based Bulk Heterojunction Solar Cells and its Impact on Device Performance. *Appl. Phys. Lett.* **2011**, *98*, 253301.
(56) He, Z. C.; Zhong, C. M.; Huang, X.; Wong, W. Y.; Wu, H. B.; Chen, L. W.; Su, S. J.; Cao, Y. Simultaneous Enhancement of Open-Circuit Voltage, Short-Circuit Current Density, and Fill Factor in Polymer Solar Cells. *Adv. Mater.* **2011**, *23*, 4636.
(57) Nardesa, A. M.; Kemerink, M.; de Kok, M. M.; Vinken, E.; Maturova, K.; Janssen, R. A. J. Conductivity, work function, and environmental stability of PEDOT:PSS thin films treated with sorbitol. *Org. Electron.* **2008**, *9*, 727.

DOI: 10.1021/am505387q
ACS Appl. Mater. Interfaces 2015, 7, 1439−1448

(58) Siddiki, M. K.; Venkatesan, S.; Galipeau, D.; Qiao, Q. Kelvin Probe Force Microscopic Imaging of the Energy Barrier and Energetically Favorable Offset of Interfaces in Double-Junction Organic Solar Cells. *ACS Appl. Mater. Interfaces* **2013**, *5*, 1279−1286.
(59) Su, Z. S.; Wang, L. D.; Li, Y. T.; Zhao, H. F.; Chu, B.; Li, W. L. Ultraviolet-Ozone-Treated PEDOT:PSS as Anode Buffer Layer for Organic Solar Cells. *Nanoscale Res. Lett.* **2012**, *7*, 1−6.
(60) Huang, J.; Miller, P. F.; Wilson, J. S.; de Mello, A. J.; de Mello, J. C.; Bradley, D. D. C. Investigation of the Effects of Doping and Post-Deposition Treatments on the Conductivity, Morphology, and Work Function of Poly(3,4-ethylenedioxythiophene)/Poly(styrene sulfonate) Films. *Adv. Funct. Mater.* **2005**, *15*, 290−296.
(61) Na, S.-I.; Wang, G.; Kim, S.-S.; Kim, T.-W.; Oh, S.-H.; Yu, B.-K.; Lee, T.; Kim, D.-Y. Evolution of nanomorphology and anisotropic conductivity in solvent-modified PEDOT:PSS films for polymeric anodes of polymer solar cells. *J. Mater. Chem.* **2009**, *19*, 9045−9053.
(62) Hwang, J.; Amy, F.; Kahn, A. Spectroscopic Study on Sputtered PEDOT Center Dot PSS: Role of Surface PSS Layer. *Org. Electron.* **2006**, *7*, 387−396.
(63) Liu, Z.; Ju, H.; Lee, E. C. Improvement of Polycarbazole-Based Organic Bulk-Heterojunction Solar Cells Using 1,8-diiodooctane. *Appl. Phys. Lett.* **2013**, *103*, 133308.

DOI: 10.1021/am505387q
ACS Appl. Mater. Interfaces 2015, 7, 1439−1448